J Neurophysiol 102: 2069–2083, 2009.
First published August 5, 2009; doi:10.1152/jn.00512.2009.

Comparison of Spatial Summation Properties of Neurons in Macaque V1 and V2

S. Shushruth,[1,*] Jennifer M. Ichida,[1,*] Jonathan B. Levitt,[2] and Alessandra Angelucci[1]

[1]*Department of Ophthalmology and Visual Science, Moran Eye Center, University of Utah, Salt Lake City, Utah; and* [2]*Department of Biology, City College of New York, New York, New York*

Submitted 12 June 2009; accepted in final form 23 July 2009

Shushruth S, Ichida JM, Levitt JB, Angelucci A. Comparison of spatial summation properties of neurons in macaque V1 and V2. *J Neurophysiol* 102: 2069–2083, 2009. First published August 5, 2009; doi:10.1152/jn.00512.2009. In visual cortex, responses to stimulation of the receptive field (RF) are modulated by simultaneous stimulation of the RF surround. The mechanisms for surround modulation remain unidentified. We previously proposed that in the primary visual cortex (V1), *near* surround modulation is mediated by geniculocortical and horizontal connections and *far* surround modulation by interareal feedback connections. To understand spatial integration in the secondary visual cortex (V2) and its underlying circuitry, we have characterized spatial summation in different V2 layers and stripe compartments and compared it to that in V1. We used grating stimuli in circular and annular apertures of different sizes to estimate the extent and sensitivity of RF and surround components in V1 and V2. V2 RFs and surrounds were twice as large as those in V1. As in V1, V2 RFs doubled in size when measured at low contrast. In both V1 and V2, surrounds were about fivefold the size of the RF and the far surround could exceed 12.5° in radius, averaging 5.5° in V1 and 9.2° in V2. The strength of surround suppression was similar in both areas. Thus although differing in spatial scale, the interactions among RF components are similar in V1 and V2, suggesting similar underlying mechanisms. As in V1, the extent of V2 horizontal connections matches that of the RF center, but is much smaller than the largest far surrounds, which likely derive from interareal feedback. In V2, we found no laminar or stripe differences in size and magnitude of surround suppression, suggesting conservation across stripes of the basic circuit for surround modulation.

INTRODUCTION

A major goal of vision research is to understand how neural circuits construct visual receptive fields (RFs). A fundamental property of RFs in early visual cortex is size tuning—i.e., a neuron's ability to respond best to a stimulus of optimal size inside its RF and to be suppressed by larger stimuli involving its RF surround (Allman et al. 1985; Blakemore and Tobin 1972; DeAngelis et al. 1994; Gilbert and Wiesel 1990; Nelson and Frost 1978). The neural circuits generating the visual cortical RF and surround are still unknown.

In the primary visual cortex (V1), RF size is larger when measured at low stimulus contrast (Kapadia et al. 1999; Sceniak et al. 1999; Sengpiel et al. 1998). We refer to the size of a high- or low-contrast stimulus evoking the largest response from a cell as the sRF_{high} and the sRF_{low}, respectively, and to the region between the sRF_{high} and the sRF_{low} as the "near" surround; we refer to the region beyond the sRF_{low} as the "far" surround.

In V1, surround suppression is fast (Bair et al. 2003) and arises far beyond the extents of geniculocortical and horizontal V1 connections (Angelucci and Sainsbury 2006; Angelucci et al. 2002), which instead are coextensive with the sRF_{high} and sRF_{low}, respectively, of their target V1 cells. Thus we proposed that feedforward and horizontal connections mediate interactions within the RF center and near surround, whereas highly divergent (Angelucci et al. 2002) and fast-conducting (Girard et al. 2001) extrastriate feedback connections to V1 generate far surround suppression (Angelucci and Bressloff 2006).

Secondary visual cortex (V2) neurons also show surround suppression (Gegenfurtner et al. 1996; Levitt et al. 1994a; Peterhans and von der Heydt 1993; Shipp and Zeki 2002a). The latter could be inherited from V1, generated de novo beyond V1, or both. V2 has the same underlying framework of circuitry as that of V1 with feedforward, horizontal, and feedback connections (reviewed in Sincich and Horton 2005). A primary difference between V1 and V2 is that V1 receives its driving input from the lateral geniculate nucleus (LGN), with modulatory input coming from cortical networks. In contrast, V2's driving input derives from V1; thus V2 is an area in which cortical input is modulated by cortical networks. We were interested in knowing whether this difference in input results in differences between V1 and V2 in how the RF is structured and/or how RF and surround components interact. Thus one major goal of this study was to perform a detailed quantitative characterization of the spatial summation properties of V2 neurons and to compare these properties with those of V1 cells recorded in the same animals.

A second goal of this study was to determine whether there are any differences in spatial summation properties among laminae or cytochrome oxidase (CO) stripe compartments in V2. Different circuits have different laminar distributions, e.g., afferent inputs terminate primarily in layers 3B–4, interareal feedback connections target the upper and lower layers, and horizontal connections are prominent in the superficial layers. Therefore to make more direct comparisons with anatomical data we have characterized the RF and surround properties of neurons in the different layers of V1 and V2. In addition, there is evidence that area V2 has anatomically and functionally specialized stripe compartments. Specifically, the different V2 stripes receive segregated inputs from V1 (Sincich and Horton 2002; Xiao and Felleman 2004; F Federer, JM Ichida, J Jeffs, I Schiessl, N McLoughlin, and A Angelucci, unpublished data) and send segregated outputs to extrastriate cortex (DeYoe and Van Essen 1985; DeYoe et al. 1994; Felleman et al. 1997;

* These authors contributed equally to this work.
Address for reprint requests and other correspondence: A. Angelucci, 65 Mario Capecchi Drive, Salt Lake City, UT 84132 (E-mail: alessandra.angelucci@hsc.utah.edu).

Nakamura et al. 1993; Shipp and Zeki 1985). Additionally, certain physiological properties of V2 cells dominate and are functionally mapped in particular stripe compartments (Chen et al. 2008; DeYoe and Van Essen 1985; Hubel and Livingstone 1987; Lu and Roe 2008; Peterhans and von der Heydt 1993; Shipp and Zeki 2002a; Tootell and Hamilton 1989; Tootell et al. 2004; Ts'o et al. 1990; Vanduffel et al. 2002; Xiao et al. 2003). However, although the anatomical connections to and from V2 support segregation of function, its intrinsic circuitry is not stripe specific (Levitt et al. 1994b) and cells across stripe types share similar response selectivity for spatial and temporal frequency, orientation, motion direction, and color (Gegenfurtner et al. 1996; Levitt et al. 1994a; Peterhans and von der Heydt 1993; Tamura et al. 1996). Other work has reported that stripe specialization is present only in the middle layers of V2, whereas the layers above and below layers 3–4 have more homogeneous response profiles (Levitt et al. 1994a; Shipp and Zeki 2002a; Shipp et al. 2009), suggesting that V2 is integrating pathway information while maintaining a segregation of outputs. We have therefore made a number of measurements of the spatial extent and sensitivity of the visual RF and surround in the different V2 stripes.

METHODS

Surgical preparation and recording

We recorded extracellularly from V1 and/or V2 of eight anesthetized (sufentanil citrate, 4–12 $\mu g \cdot kg^{-1} \cdot h^{-1}$) and paralyzed (vecuronium bromide, 0.1 $\mu g \cdot kg^{-1} \cdot h^{-1}$) macaque monkeys (*Macaca fascicularis*). All procedures conformed to the guidelines of the University of Utah Institutional Animal Care and Use Committee. Animals were artificially respirated with a 30:70 mixture of O_2 and N_2O. The electrocardiogram was continuously monitored, end-tidal CO_2 was maintained at 30–33 mmHg, rectal temperature was near 37°C, and blood oxygenation was near 100%. The pupils were dilated with topical atropine and the corneas protected with rigid gas-permeable contact lenses. The locations of the foveae were plotted at the beginning of the experiment and periodically thereafter, using a reversible ophthalmoscope. Supplementary lenses were used to focus the eyes on the display screen.

Single-unit recordings were made with epoxylite-coated tungsten microelectrodes (4–6 MΩ; FHC, Bowdoin, ME). Spikes were conventionally amplified, filtered, and sampled at 22 kHz by a dual-processor G5 Power Macintosh computer running custom software (EXPO), kindly donated to us by Dr. Peter Lennie. Spikes were displayed on a monitor and templates for discriminating spikes were constructed by averaging multiple traces. The timing of waveforms that matched the templates was recorded with an accuracy of 0.1 ms.

Visual stimuli and characterization of receptive fields and surround fields

Sinusoidal gratings of the same mean luminance as that of the background were generated by the same software and computer that recorded spikes and were displayed on a calibrated monitor (Sony GDM-C520K), refreshed at 100 Hz, of mean luminance approximately 45.7 cd/m^2, at a viewing distance of 57 cm (at which the screen subtended a visual angle of 28°). For each cell, we first determined the preferred orientation, drift direction, and both spatial and temporal frequencies. Then the area and center of the minimum response field (mRF) were carefully located quantitatively using a grating patch of 0.1° radius for V1 cells and 0.1–0.3° radius for V2 cells. The area of the mRF was defined as the visual field region in which the small grating patch elicited a response ≥2SD above the cell's spontaneous rate. The mRF diameter was calculated as the square root of this area and this area's geometric center was defined as the mRF center. Using a grating patch matched to the cell's mRF diameter, we generated a contrast response function for each cell and used the individual cell responses to tailor the contrast values for the remaining stimuli. High-contrast values were chosen so neuronal responses did not exceed 90% of the maximal response for the cell (typically 50–80% contrast); low-contrast values were generally chosen to be those eliciting <50% of the maximum response in the individual cell's contrast–response function, but still eliciting a reliable response (≥2SD greater than the spontaneous firing rate; typically 4–30% contrast).

RF AND SURROUND SIZE MEASURED BY THE EXPANDING PATCH METHOD. We performed spatial summation measurements at two contrast levels (high and low), using circular patches of drifting gratings of increasing radius centered over the cell's mRF. The patch radius ranged from 0.1 to 14° and consisted of 11 radii presented in random order within each block of trials. From these patch-size tuning curves at high and low contrasts, for each cell we extracted as a measure of RF size the patch radius at peak response (i.e., the radius of the sRF_{high} and sRF_{low}, respectively). The latter were then used to create the center and annular surround stimuli used for the "expanding annulus method" described in the following text. From the patch-size tuning curves, we also extracted as a measure of surround size the patch radius at asymptotic response.

SURROUND SIZE MEASURED BY THE EXPANDING ANNULUS METHOD. In this experimental protocol, the visual stimulus consisted of a high-contrast center grating the radius of the cell's sRF_{high}, surrounded by a high contrast annular grating of fixed outer radius (14°) and an inner radius whose size was decreased from 12.5° to a size ≥ the sRF_{low} of the cell (we used nine annulus inner radii). Thus there was always a blank annulus of the same luminance as that of the background interposed between the center grating patch and the surround annular grating (i.e., covering the near surround).

Control conditions included a blank screen (of the same luminance as that of the background) for a measure of spontaneous activity, a center-alone condition for a baseline response, and a surround annulus-alone condition to ensure that the annular surround stimulus alone did not drive a response.

Both annular and patch stimuli were presented randomly in a blockwise fashion with a duration of 2 s and a 2 s interstimulus interval. Each block was repeated 10 times and the responses across blocks were averaged to calculate the mean firing rate for each stimulus condition.

Histology and track reconstruction

Electrolytic lesions (1 μA for 30–40 s, tip negative) were made along the length of each electrode penetration to assign laminar location and CO stripe type to recorded V1 and/or V2 neurons. Our electrode penetrations were angled approximately orthogonal to the pial surface. At the end of the recording session the animal was killed with sodium pentobarbital and perfused transcardially with saline, followed by 4% paraformaldehyde for 15 min. In six cases, areas V1 and V2 were dissected away from the rest of the brain, flattened between glass slides, postfixed for 1–2 h, cryoprotected, and frozen sectioned at 40 μm tangentially to the pial surface. In two cases, in which recordings were made only from V1, the brain was blocked on a plane parallel to the electrode tracks and then sectioned at 40 μm parallel to that plane (i.e., in a near-to-coronal plane). In the latter two cases, alternate sections were stained for Nissl or CO, whereas in the tangentially sectioned brains all sections were reacted for CO. Electrode tracks were reconstructed by drawing lesions on each individual section using a camera lucida attached to a light microscope and individual sections were aligned using vascular landmarks as fiducial

marks. Laminar locations of lesions and recording tracks were determined on CO and Nissl sections. To identify the V2 CO stripes, CO staining in tangential sections was visualized at low magnification (×1.25) and digitized using a camera mounted onto a Zeiss light microscope and image analysis software (Image Pro Plus; Media Cybernetics, Silver Spring, MD). For each case up to eight serial CO-stained tissue sections were overlaid by aligning the radial blood vessels and merged in Adobe Photoshop. We find that the stripe pattern is much clearer in these composite CO images than in any single CO section. CO stripes were identified on these composite images and the reconstructions of the lesions and electrode tracks were superimposed on these CO images using the radial blood vessels for alignment (Fig. 1). Thick and thin stripes were identified by their relative width and alternation. Although absolute width is a poor indicator of stripe type, the regular alternation in relative width is a useful criterion to identify stripes. Because stripe borders are blurry and cannot be determined with a precision greater than ±100 μm, we classified cells located within about 100 μm of a stripe border as "border" cells.

Data analysis and statistical model fitting

The patch-size tuning data were fit with the difference of the integral of two Gaussian functions (DOGs; Sceniak et al. 1999, 2001). The annulus-size tuning data were instead fit with a "thresholded difference of Gaussians" (t-DOG) model, as previously described (Ichida et al. 2007). Briefly, the t-DOG model describes excitation and inhibition as two Gaussians of identical spatial scales, with the inhibition becoming effective after a threshold is crossed. The values of the free parameters in both models were optimized to produce the best least-squares fit to the data. In RESULTS, we report the analysis based on these statistical model fits. Statistical tests used to determine significance are reported in RESULTS. Descriptive cell population statistics for the measured parameters are reported in Tables 1 and 2.

A cluster analysis was performed on the V2 cell data pooled across stripe types to test for clustering of the measured physiological response properties, independent of our CO stripe assignment. Using custom Matlab scripts, for each parameter examined we calculated within-cluster Euclidean distance and then calculated linkage using Ward's method. A Thorndike procedure was used to estimate the likely number of distinct clusters in the data for that parameter (Briggs and Callaway 2005; Cauli et al. 2000; Thorndike 1953).

RESULTS

We recorded from 79 single units in foveal (n = 5 cells at <2° eccentricity) and parafoveal (2–7° eccentricity) V1 and 91 units in foveal (n = 11 cells at <2° eccentricity) and parafoveal V2 (2–10°). Our V1 sample included cells from all layers; our V2 sample included cells in layers 3–6. Most cells in our V1sample had complex RFs (n = 70 of 79 cells); therefore in the analysis we make no distinction between simple and complex RFs. Cells in V2 were sampled from all stripe types (n = 40 in thick, 14 in thin, and 16 in pale stripes; 7 cells were located at stripe borders; for 14 cells stripe location could not be determined). Previous studies in New and Old World monkeys indicated that pale stripes located medially and laterally, respectively, to thick stripes may be functionally (Roe and Ts'o 1995; Shipp and Zeki 2002a; Xu et al. 2004) and

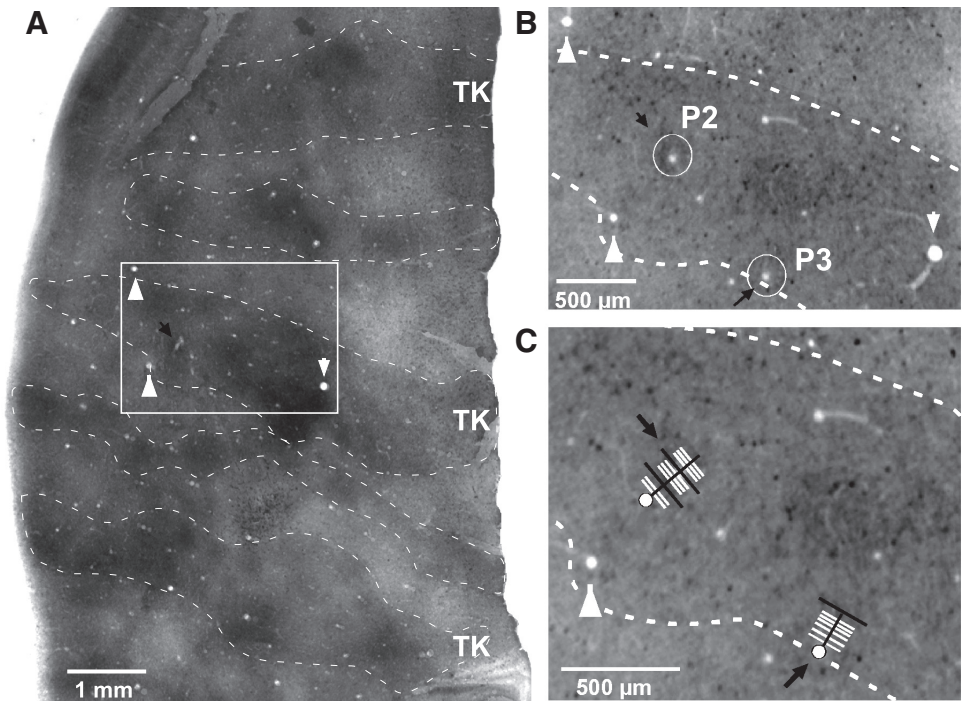

FIG. 1. Example of 2 reconstructed electrode penetrations in secondary visual cortex (V2). *A*: low-power view of a portion of area V2 stained for cytochrome oxidase (CO), showing alternating thick (TK), pale, and thin CO stripes (dashed contours outline the dark CO stripes). The image is a composite of 4 CO sections that were aligned and merged using Adobe Photoshop. Two electrode penetrations are located inside the boxed area, which is shown at higher power in *B*. The black arrow points at one visible electrolytic lesion that was located along electrode penetration 2 (P2). Lesions placed along penetration 3 (P3) are not visible in this composite low-power image because they were either located in sections not used to make the composite CO image or because they were located in only one of the sections used for the composite image. White arrowheads in *A* point at the same blood vessel profiles as in *B* and *C*. *B*: higher-power view of a single CO-stained section inside the boxed region in *A* (used for the composite image in *A*) showing 2 lesions (circled and marked by black arrows), one along P2, the other along P3. *C*: higher-power view of the same section as in *B* showing the location of the 2 electrode penetrations (black arrows). White segments indicate the location of recorded cells. Black segments indicate locations of lesions and recorded cells (2 along P2 and one along P3). White dots indicate locations of lesions only (no cells recorded). Notice that all recorded cells in P2 and P3 were located in a thick CO stripe.

anatomically (Federer et al., unpublished data) distinct. Since most cells in our V2 pale stripe sample were from pale-lateral stripes ($n = 12$ of 16 cells), we did not make a distinction in the analysis between pale-lateral and pale-medial stripes. For each unit we initially determined the optimal orientation, spatial and temporal frequencies, and the radius and center of the mRF. Mean and median mRF diameters in V1 were 0.3 ± 0.13° (SD) and 0.22°, respectively (range, 0.13–0.84°); in V2 mean mRF was 0.52 ± 0.12° and median mRF was 0.49° (range, 0.34–2.31°). We next measured the spatial extent over which responses in V1 and V2 summated (i.e., the size of the sRF).

Summation receptive field sizes

The sRF size was measured using the expanding patch method—i.e., by increasing the radius of a circular grating patch centered over the cell's mRF and measuring response amplitude as a function of the patch radius. Figure 2 shows patch-size tuning curves for three example V1 (Fig. 2, *A–C*) and three example V2 (Fig. 2, *D–F*) cells measured at high and low stimulus contrast. In both V1 and V2, responses increased with stimulus radius up to a peak and either asymptoted at the peak (e.g., Fig. 2, *C* and *F*) or were suppressed as stimulus size was further increased (e.g., Fig. 2, *A* and *B* and *D* and *E*). For cells that showed suppressive surrounds, the sRF size was defined as the stimulus radius at peak response, extracted from the DOG model fits to the size tuning data. For cells that showed no suppressive surrounds, instead, the sRF size was defined as the stimulus radius at which the response reached 95% of its maximum value, again extracted from the DOG model fits to the data.

Figure 3, *A* and *B* shows for our cell samples the distribution of sRF sizes at high and low contrast in V1 and V2, respectively. This parameter was more narrowly distributed in V1 (mean sRF_{high}: 0.36 ± 0.13°) than in V2 (mean sRF_{high}: 0.74 ± 0.5°). Under both contrast conditions, sRF sizes were significantly larger in V2 than those in V1 ($P < 0.001$, Mann–Whitney *U* test). Population mean and median values for sRF sizes in V1 and V2 are reported in Table 1. In addition, for most V1 and V2 cells the sRF was larger when measured at low contrast. At the population level, this contrast-dependent sRF expansion was statistically significant for both V1 and V2 ($P < 0.01$ for both, Mann–Whitney *U* test). This phenomenon was previously reported for V1 cells (Cavanaugh et al. 2002; Ichida et al. 2007; Sceniak et al. 1999; Sengpiel et al. 1998), but not for V2 cells. The ratio of the sRF_{low} to the sRF_{high}, estimated cell by cell, averaged 1.65 ± 0.72 in V1 and 1.57 ± 0.73 in V2 (Fig. 3, *C* and *D*; Table 1). The distributions of these sRF ratios in V1 and V2 were statistically indistinguishable ($P = 0.43$, ANOVA).

Figure 4*A* shows the distribution of sRF radii across the V1 layers. We found very little laminar variation and no statistically significant difference in sRF size across V1 layers ($P = 0.45$ and 0.57 for sRF_{high} and sRF_{low}, respectively; Kruskal–Wallis test). Consistent with previous reports (Sceniak et al. 1999), the distribution of the sRF_{low}/sRF_{high} ratio also did not differ significantly across layers. However, there was a tendency for smaller ratios to be in layers 2–3A and 6 (Fig. 4*B*).

In V2, the overall population of sRF sizes (pooled across CO stripes) at both high (Fig. 4*C*) and low contrast (Fig. 4*D*) did not show any statistically significant laminar distribution, de-

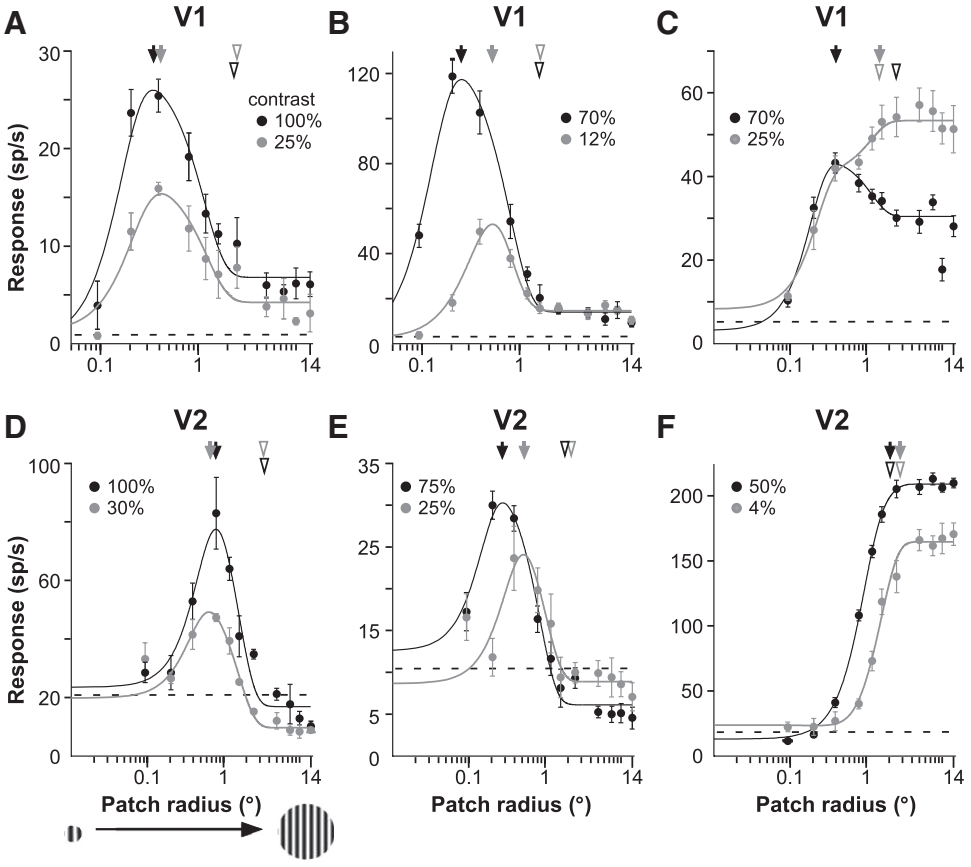

FIG. 2. Patch-size tuning curves for 3 example V1 cells and 3 example V2 cells. Responses (mean firing rate) of 3 V1 cells (*A–C*) and 3 V2 cells (*D* and *E*) as a function of the radius of a circular optimal grating patch (stimulus shown in *D*). Black and gray curves: responses to a high- or low-contrast stimulus, respectively (contrast values used are indicated in each panel). Solid lines represent fits to the data (dots) using the difference of Gaussians (DOGs) model (see METHODS). Dashed lines indicate the cell's mean spontaneous firing rate. Arrows: radius of the high- or low-contrast stimulus evoking the largest response from a cell, respectively, sRF_{high} (black) and sRF_{low} (gray): 0.35 and 0.42° (*A*), 0.26 and 0.54° (*B*), 0.42 and 1.44° (*C*), 0.8 and 0.65° (*D*), 0.28 and 0.53° (*E*), 2.02 and 2.73° (*F*). Open arrowheads: surround sizes, i.e., stimulus radius at asymptotic response, measured at high (black) and low (gray) stimulus contrast: 2.03 and 2.18° (*A*), 1.41 and 1.41° (*B*), 2.1 and 1.44° (*C*), 2.89 and 2.83° (*D*), 1.53 and 1.87° (*E*), 2.02 and 2.73° (*F*). Error bars represent SE values. The suppression index (SI) at high stimulus contrast for each cell was: 0.7 (*A*), 0.84 (*B*), 0.28 (*C*), 0.74 (*D*), 0.76 (*E*), 0 (*F*).

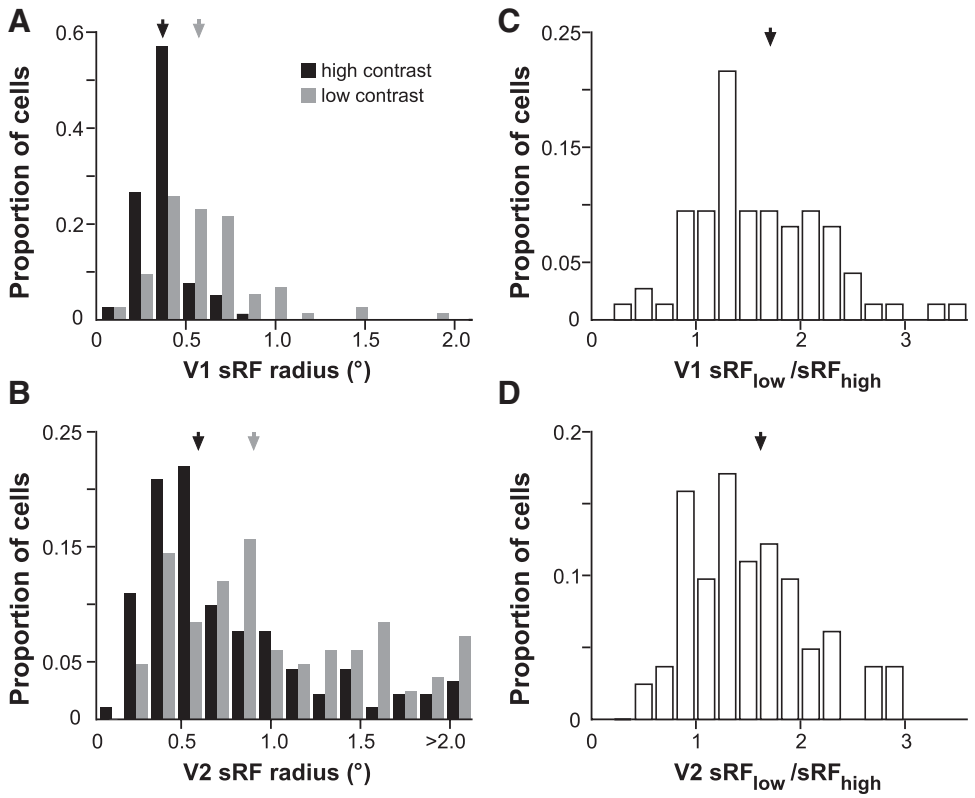

FIG. 3. sRF sizes in V1 and V2: population data. *A* and *B*: distribution of sRF_{high} (black bars) and sRF_{low} (gray bars) radii in V1 (*A*) and V2 (*B*). Black and gray arrows: median sRF_{high} and sRF_{low}, respectively; see Table 1 for values. *C* and *D*: distribution of the sRF_{low}/sRF_{high} ratio, computed on a cell-by-cell basis, in V1 (*C*) and V2 (*D*). A ratio >1 indicates that the sRF is larger at low than at high contrast. Arrows: median ratio. Note similarity of the V1 and V2 distributions and their respective median values.

spite a tendency for sRF sizes to be larger in layer 6 (median sRF_{high} values in layers 3, 4, and 6 were 0.73, 0.78, and 0.83°, respectively). However, small and large sRF sizes could be found in all layers.

sRF sizes were also statistically homogeneous across CO stripe compartments in V2, albeit there was a statistically nonsignificant ($P = 0.09$, Kruskal–Wallis test) tendency for larger and smaller sRF sizes to be found in thin (mean sRF_{high} radius: 0.81 ± 0.51°) and pale (mean sRF_{high} radius: 0.51 ± 0.22°) stripes, respectively. The pale stripes showed the narrowest spread in sRF_{high} sizes, whereas the thick stripes (mean sRF_{high} radius: 0.77 ± 0.53°) showed the largest spread. The descriptive statistics for sRF sizes at high and low contrast across the population of V2 cells grouped by CO stripe type are reported in Table 2. In Table 2 we report only cells ($n = 70$) that were located within a single stripe type (i.e., border cells are not reported in the table, nor are cells for which the stripe location could not be determined).

As in V1, in V2 the distribution of the sRF_{low}/sRF_{high} ratio did not show any significant laminar variation, nor was there any significant difference in ratio across different stripe types (Fig. 4*E*).

TABLE 1. *Descriptive statistics for V1 and V2 cell populations, pooled across layers and stripes*

Parameter	Mean ± SD	Median	Range	*n*	Figure
		A. V1 cells			
sRF_{high} radius	0.36 ± 0.13	0.34	0.11–0.82	79	3A
sRF_{low} radius	0.60 ± 0.34	0.54	0.25–1.99	75	3A
sRF_{low}/sRF_{high}	1.65 ± 0.72	1.54	0.26–3.43	75	3C
Surround radius at high contrast [patch]	1.62 ± 0.62	1.59	0.55–2.66	79	5A
Surround radius at low contrast [patch]	1.87 ± 1.05	1.70	0.41–3.48	67	5A
Far surround radius at high contrast [annulus]	5.52 ± 2.64	4.65	2.45–>12.5	44	8A
SI [patch]	0.58 ± 0.17	0.63	0.24–0.87	79	10A
SI [annulus]	0.25 ± 0.17	0.25	0.0–0.61	55	10A
		B. V2 cells			
sRF_{high} radius	0.74 ± 0.50	0.56	0.16–2.43	91	3B
sRF_{low} radius	1.04 ± 0.68	0.87	0.18–3.55	83	3B
sRF_{low}/sRF_{high}	1.57 ± 0.73	1.44	0.47–2.98	83	3D
Surround radius at high contrast [patch]	3.56 ± 1.94	2.85	1.06–10.55	83	5B
Surround radius at low contrast [patch]	3.85 ± 2.31	3.40	0.84–11.65	75	5B
Far surround radius at high contrast [annulus]	9.24 ± 2.91	9.46	3.11–>12.5	69	8B
SI [patch]	0.54 ± 0.23	0.59	0.0–0.90	91	10B
SI [annulus]	0.25 ± 0.20	0.24	0.0–0.64	78	10B

Surround sizes

The extent of the suppressive surround was measured using two different stimulus protocols: the expanding patch method and the expanding annulus method described in detail in METHODS. Data obtained using these two different protocols are described separately in the following text.

SURROUND SIZE MEASURED BY THE EXPANDING PATCH METHOD. In addition to the RF center, this stimulus protocol activates all surround regions, i.e., both near and far (stimulus shown in Fig. 2*D*). However, we have previously shown that in V1 it reveals predominantly the stronger modulatory effects of near surround stimulation (Ichida et al. 2007; Levitt and Lund 2002).

Using this stimulus, the surround radius was defined as the grating patch radius at which the cell's response asymptoted—

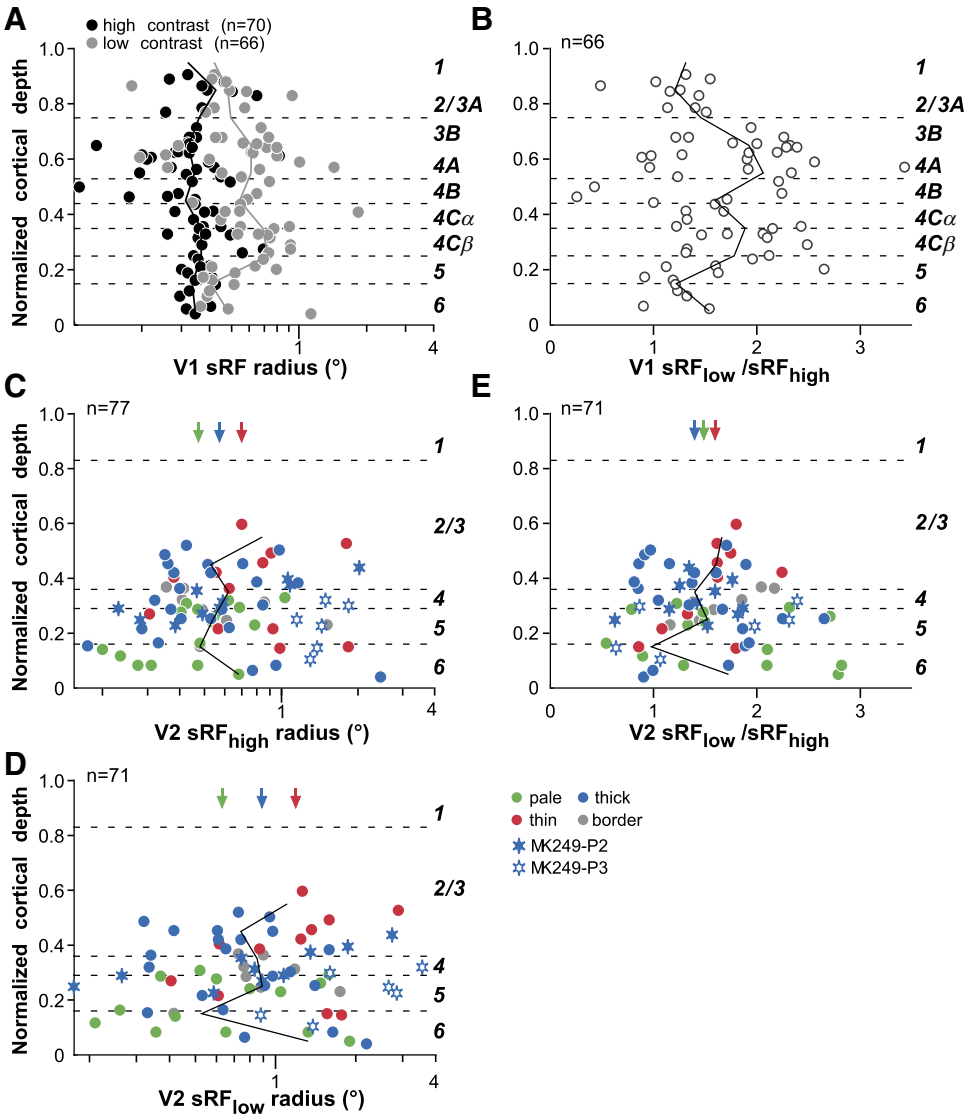

FIG. 4. Laminar distribution of sRF sizes in V1 and in different V2 CO stripes. *A*: laminar distribution of the sRF$_{high}$ (black symbols) and sRF$_{low}$ (gray symbols) radii vs. cortical depth for the V1 cell population. Here and in *B–E* the dashed horizontal lines mark the cortical layer boundaries and the cortical layers are indicated to the *right* of the plots. Solid black and gray lines: median sRF$_{high}$ and sRF$_{low}$ radius, respectively, of the V1 cell sample calculated at intervals of 10% of total cortical depth. *B*: laminar distribution of the sRF$_{low}$/sRF$_{high}$ ratio in V1. Solid line: median ratio at intervals of 10% of total cortical depth. *C–E*: laminar distribution of the sRF$_{high}$ (*C*), sRF$_{low}$ (*D*), and sRF$_{low}$/sRF$_{high}$ ratio (*E*) in V2. Cells are color coded according to stripe type location (as indicated in the legend). In gray are the border cells, i.e., those located within 100 μm of the border between 2 stripe types (thick/pale or thin/pale). Filled and open blue stars indicate cells recorded along the electrode penetrations 2 (P2) and 3 (P3), respectively, shown in Fig. 1, both located in a thick CO stripe. Solid line: median values calculated at intervals of 10% of total depth for all cells pooled across stripe types. Arrows: median values (reported in Table 2) calculated for all cells within a stripe group, pooled across cortical layers.

i.e., had fallen to 5% of the difference between the peak response and the response to the largest stimulus used (open arrowheads in Fig. 2). These values were derived from the DOG model fits to the patch-size tuning data. Figure 5, *A* and *B* shows the distribution of surround radii at high and low contrast in V1 and V2, respectively; we excluded from these histograms cells whose asymptotic response coincided with the peak response in the high-contrast patch-size tuning curve (i.e., cells that were not surround suppressed). As shown in *Strength of surround suppression*, in V1 we found no cells whose response, measured at high stimulus contrast, asymptoted at the peak response; therefore by this criterion, all V1 cells in our sample were suppressed by large grating patches and are thus included in the histogram of Fig. 5*A*. In V2, only 8 of 91 cells were not surround suppressed by high-contrast grating patches of 14° radius (one example is shown in Fig. 2*F*); these cells are thus not included in the histogram of Fig. 5*B*. In both V1 and V2, we found no statistically significant difference between surround sizes measured using grating patches of high or low contrast ($P = 0.24$ and 0.68, respectively, Mann–Whitney *U* test), although in both areas there was a tendency for surrounds to be larger at low contrast (Fig. 5, *A* and *B*; Table 1). Surround radius was much more narrowly distributed in V1 (mean at high contrast, 1.62 ± 0.62°) than that in V2 (mean at high contrast, 3.56 ± 1.94°) (Table 1). In V1, surround radius at high contrast ranged from 0.55 to 2.7° and about half of the V1 sample had response asymptotes at stimulus radii >1.5°. V2 surrounds measured at high contrast ranged from 1.1 to 10.6° and about half of the V2 sample had surround radii >3°. In summary, V2 surrounds were about twice as large as V1 surrounds and this difference was statistically significant ($P < 0.001$, Mann–Whitney *U* test). In addition, multiplying V1 surround sizes by a factor of 2 yielded a distribution that was statistically indistinguishable from the distribution of V2 surround sizes ($P = 0.21$, Kolmogorov–Smirnov [K-S] test; $P = 0.99$, Mann–Whitney *U* test).

Surround radius measured at high stimulus contrast was linearly correlated with the radius of the sRF$_{high}$ in both V1 and V2 (Fig. 5, *C* and *D*; $r = 0.39$ and 0.56, respectively; $P < 0.001$ for both V1 and V2, Pearson's correlation), indicating that cells with larger sRF sizes also had larger surround field sizes. The ratio of surround radius (at high contrast) to sRF$_{high}$ radius calculated cell by cell averaged 5.73 ± 3.42 (median, 4.96; range, 1–17.9) in V1 and 4.72 ± 1.76 (median, 4.57;

TABLE 2. *Descriptive statistics for V2 cell populations in different stripe types*

Parameter	Mean ± SD	Median	Range	*n*	Figure
A. Thick stripes					
sRF_{high} radius	0.77 ± 0.53	0.58	0.17–2.43	40	4C
sRF_{low} radius	1.11 ± 0.80	0.89	0.18–3.56	39	4D
sRF_{low}/sRF_{high}	1.46 ± 0.51	1.41	0.63–2.65	39	4E
Surround radius at high contrast [patch]	3.56 ± 2.06	2.89	1.06–10.55	40	6B
Surround radius at low contrast [patch]	3.25 ± 1.50	2.83	1.45–6.61	39	6C
Far surround radius at high contrast [annulus]	8.61 ± 2.75	8.81	3.15–12.46	38	8D
SI [patch]	0.57 ± 0.21	0.62	0.0–0.88	40	11B
SI [annulus]	0.28 ± 0.15	0.26	0.0–0.64	38	11C
B. Thin stripes					
sRF_{high} radius	0.81 ± 0.51	0.70	0.15–1.82	14	4C
sRF_{low} radius	1.29 ± 0.70	1.26	0.41–2.89	11	4D
sRF_{low}/sRF_{high}	1.94 ± 1.27	1.62	0.86–2.24	11	4E
Surround radius at high contrast [patch]	3.50 ± 1.25	3.71	1.80–5.61	14	6B
Surround radius at low contrast [patch]	4.53 ± 3.38	3.78	1.12–11.65	11	6C
Far surround radius at high contrast [annulus]	8.79 ± 2.69	9.35	3.11–11.66	14	8D
SI [patch]	0.48 ± 0.25	0.52	0.0–0.78	14	11B
SI [annulus]	0.23 ± 0.30	0.15	0.0–0.57	14	11C
C. Pale stripes					
sRF_{high} radius	0.51 ± 0.22	0.48	0.20–1.00	16	4C
sRF_{low} radius	0.82 ± 0.55	0.63	0.21–1.90	14	4D
sRF_{low}/sRF_{high}	1.70 ± 0.76	1.49	0.54–2.82	14	4E
Surround radius at high contrast [patch]	3.35 ± 1.57	2.64	1.40–7.15	16	6B
Surround radius at low contrast [patch]	3.71 ± 2.20	3.02	0.84–7.44	14	6C
Far surround radius at high contrast [annulus]	10.12 ± 2.18	10.35	6.15–>12.5	16	8D
SI [patch]	0.63 ± 0.16	0.60	0.40–0.90	16	11B
SI [annulus]	0.21 ± 0.18	0.23	0.0–0.64	16	11C

range, 2.1–11.2) in V2. Thus both in V1 and V2 surround size was about fivefold larger than the RF center size.

Figure 6*A* shows that surround size (patch radius at asymptotic response) in V1, like sRF size, did not have any particular laminar distribution; cells with both large and small surrounds could be found in all V1 layers and no laminar differences were statistically significant ($P = 0.84$, Kruskal–Wallis test). In V2 (Fig. 6, *B* and *C*), the overall population of surround sizes (pooled across stripe types) showed a slight tendency for surrounds to be smaller in the input layers (deep 3B and 4); median high-contrast surround radius in layers 3B and 4 (pooled together) was 2.7° (mean ± SD: 3.2 ± 1.71°) versus 3.4° (mean ± SD: 3.9 ± 2.52°) in layer 5 and 3.2° (mean ± SD: 3.9 ± 2.07°) in layer 6. However, this trend was statistically nonsignificant ($P = 0.32$, Kruskal–Wallis test).

We found no difference in surround sizes across CO stripe types ($P = 0.64$). Mean surround radius at high contrast was 3.5 ± 1.25° for thin stripes, 3.56 ± 2.1° for thick stripes, and 3.35 ± 1.6° for pale stripes (see Table 2). We found only few cells with no surround suppression (cells with 0° surround radius in Fig. 6*B*) at high contrast in the thick and thin stripes and no cells that did not suppress in the pale stripes.

SURROUND SIZE MEASURED BY THE EXPANDING ANNULUS METHOD. In this stimulus protocol, the RF center was stimulated by a high-contrast grating patch of optimal stimulus parameters for the recorded cell fitted to the radius of the cell's sRF_{high}. The surround was simultaneously stimulated with a high-contrast annular grating of 14° outer radius and an inner radius that was systematically decreased from 12.5° to a size ≥ cell's sRF_{low} (stimulus shown in Fig. 7*C*); the annular grating had stimulus parameters identical to those of the center grating because, at least in V1, the sRF_{low} is on average coextensive with the spread of monosynaptic horizontal connections (Angelucci et al. 2002); this stimulus protocol allowed us to minimize afferent stimulation of the near surround and to isolate the weaker modulatory signals from the far surround. The latter is the surround region beyond the extent of monosynaptic horizontal connections, which we have proposed to be mediated by extrastriate feedback connections to V1 (Angelucci and Bressloff 2006) (see INTRODUCTION).

Annulus-size tuning curves for two example V1 cells and two example V2 cells are shown in Fig. 7, *A* and *B* and *C* and *D*, respectively. In both V1 and V2, as the inner radius of the annular grating was decreased—i.e., as more of the far surround region was stimulated (read the *x*-axes in Fig. 7 from right to left)—the cell's response was suppressed. From the t-DOG fits to the annulus-size tuning data we extracted, as a measure of far surround radius, the annular grating's inner radius at onset of suppression (i.e., at which responses had fallen 10% or 1SE below the center-only response, whichever was lower; arrows in Fig. 7). In cases in which the largest annulus inner radius used (as limited by the display screen size) caused stronger suppression than this criterion, the surround radius was considered to be >12.5° (e.g., Fig. 7*C*).

Figure 8, *A* and *B* shows the distribution of far surround radii, measured at high stimulus contrast in V1 and V2, respectively. We excluded from the histograms cells that did not show far suppressive surrounds (i.e., whose center-only response was not suppressed by ≥10% or 1SE), i.e., 22% of cells in V1 and 17% in V2. In both V1 and V2 far surround radii could be >12.5° (the largest values were limited by our display screen size), but in V1 far surround radius averaged 5.5 ± 2.64°, whereas in V2 it averaged 9.2 ± 2.9° (Table 1). Furthermore, about half of the V1 cells had far surround radii >3°, whereas about half of the V2 sample showed far surround radii >9°. In summary, V2 far surrounds were about twice as large as V1 far surrounds and this difference was statistically significant ($P < 0.001$, Mann–Whitney *U* test). Furthermore, multiplying V1 far surround radii by a factor of 2 again yielded a distribution that was statistically indistinguishable from the distribution of V2 far surround sizes ($P = 0.16$, K-S test; or $P = 0.35$, Mann–Whitney *U* test).

Figure 8*C* shows, as we previously reported (Ichida et al. 2007), that far surround radii (annulus inner radius at suppression onset) in geniculocortical-recipient layer 4C of V1 were significantly smaller than those in other V1 layers ($P = 0.02$, Kruskal–Wallis test). Far surround radius ranged from 2.7 to 7.2° in layer 4C (median: 4.3°), whereas it could reach >12.5° in the upper layers (median in layers 2/3: 5.2°).

In contrast to V1, far surround sizes in V2 did not show any statistically significant differences among cortical layers or CO stripes (Fig. 8*D*) and cells with no far surround suppression (i.e., whose center-only response was not suppressed by adding

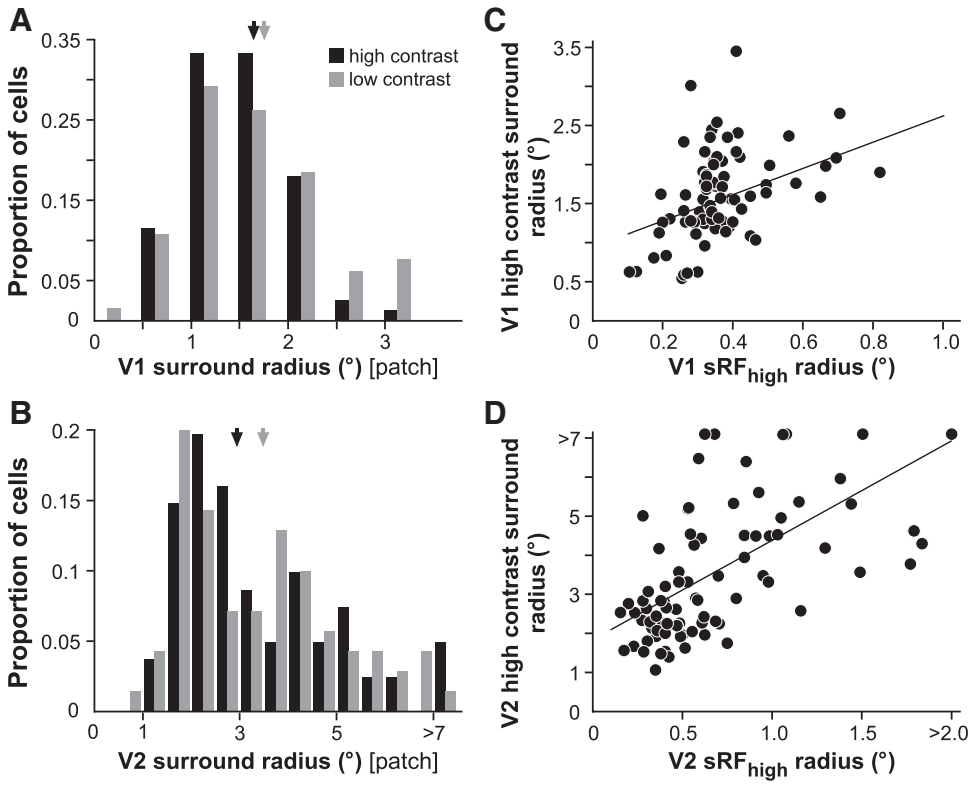

FIG. 5. Surround sizes in V1 and V2 measured with expanding patch method. *A* and *B*: distribution of surround radii (asymptotic response radii) measured at high (black bars) and low (gray bars) stimulus contrast for the V1 (*A*) and V2 (*B*) cell samples. Black and gray arrows indicate median values at high and low contrast, respectively; see Table 1 for values. *C* and *D*: scatterplots of the sRF_{high} radius vs. the surround radius measured at high contrast for the V1 and V2 cell samples, respectively. Black lines: regression lines. Note that the *x*-axes in *B* and *D* are exactly twice those in *A* and *C*, respectively.

an annular surround stimulus of inner radius equal to the cell's sRF_{low}) were seen in all V1 and V2 layers as well as in all CO stripes. Compared with thick (mean: 8.6 ± 2.75°) and thin (mean: 8.8 ± 2.69°) CO stripes, far surround radii in the pale stripes (mean: 10.1 ± 2.18°) were more narrowly distributed and showed a statistically nonsignificant tendency to be larger (Table 2).

For most V1 and V2 cells, surround size measured using the expanding annulus method was much larger than when measured using the expanding patch method (Table 1 and Fig. 9). This is because the strength of surround suppression is maximal closer to the RF center; therefore masking out the near surround reveals more distant surround influences (see the next subsection; see also L Schwabe, JM Ichida, S Shushruth, and A Angelucci, unpublished data). This is also evident when comparing the slopes of the response functions in Fig. 2, *A* and *B* and *D* and *E* with those in Fig. 7, *A* and *B* and *C* and *D*, respectively; responses in Fig. 7 show shallower slopes than those in Fig. 2. The ratio of far surround radius measured with annulus to surround radius measured with patch was similar in V1 and V2 (medians in V1 = 3.07, in V2 = 2.84; $P = 0.54$, Mann–Whitney *U* test; Fig. 9, *A* and *B*). These two measures of surround radius were not significantly correlated in V1 or V2 ($r = 0.27$, $P = 0.07$, in V1; $r = -0.11$, $P = 0.38$ in V2; Pearson's correlation; Fig. 9, *C* and *D*), perhaps suggesting different underlying anatomical substrates. There were no statistical differences in surround ratios among layers or stripes.

Strength of surround suppression

From the patch-size tuning data, we calculated as a measure of suppression strength, a suppression index [$SI_{patch} = 1 -$ (response at largest patch size/peak response)]. The strength of far surround suppression was instead measured from the annulus-size tuning data as: $SI_{annulus} = 1 -$ (response at the annular grating's smallest inner radius/center-only response). A SI of 0 indicates complete lack of suppression, whereas a SI of 1 indicates that the cell's response was completely suppressed by the largest patch or annular surround gratings.

In both V1 and V2, suppression strength induced by the grating patch was significantly stronger than the strength of far surround suppression induced by the annular grating ($P < 0.001$ in both areas, Mann–Whitney *U* test; Fig. 10). In V1 the SI_{patch} ranged from 0.24 to 0.87 (mean: 0.58 ± 0.17), whereas the $SI_{annulus}$ ranged from 0 to 0.61 (mean: 0.25 ± 0.17). Similarly, in V2 SI_{patch} ranged from 0 to 0.9 (mean: 0.54 ± 0.23) and $SI_{annulus}$ ranged from 0 to 0.64 (mean: 0.25 ± 0.2) (Table 1). In contrast to previous studies, in V1 we found no cells that were not surround suppressed by the largest high contrast grating patch used (see DISCUSSION); the smallest SI in V1 was 0.24. In contrast, 22% of cells in V1 showed no far surround suppression, i.e., they were not suppressed by the largest annular surround grating used; all these cells, however, were suppressed by large grating patches (Fig. 10, *A* and *C*). In V2, for only eight cells the $SI_{patch} = 0$, and for 10% of cells ($n = 9$) it was <0.2; many more V2 cells (17%) showed no far surround suppression, but at least half of them could be suppressed by large grating patches (Fig. 10, *B* and *D*).

Distributions of SIs (both SI_{patch} and $SI_{annulus}$) in V1 were statistically indistinguishable from those in V2 ($P = 0.66$ for SI_{patch} and 0.95 for $SI_{annulus}$; K-S test). Furthermore, in both V1 and V2, these two measures of surround suppression strength were significantly correlated ($r = 0.58$ in V1 and 0.59 in V2, $P < 0.001$ in both areas, Pearson's correlation; Fig. 10, *C* and

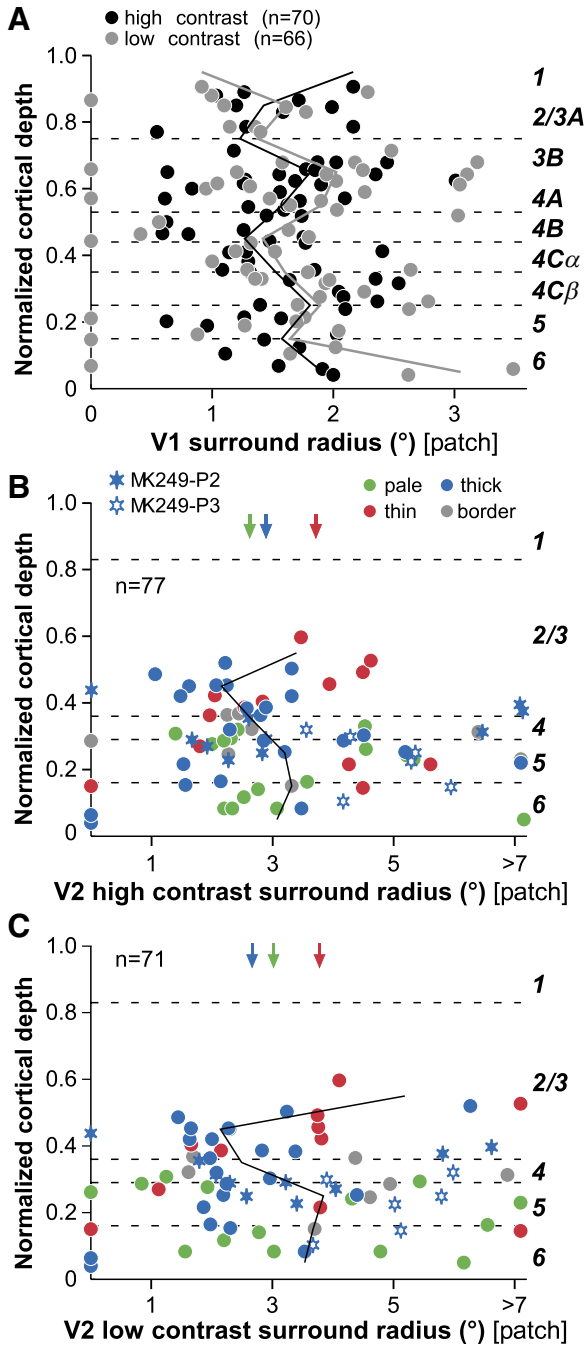

FIG. 6. Laminar distribution of surround sizes in V1 and in V2 CO stripes, measured with expanding patch method. *A*: laminar distribution of surround radius at high (black symbols) and low (gray symbols) stimulus contrast for the V1 cell population. *B* and *C*: laminar distribution of surround radius at high (*B*) and low (*C*) contrast for the V2 cell population. Solid lines indicate median surround radius calculated at intervals of 10% total cortical depth. Cells that showed no surround suppression are indicated on the *y*-axes as cells having surround radii = 0°. These cells were not included in the calculation of the median values. Other conventions are as in Fig. 4. Note that the *x*-axes both in *A* and in *B* and *C* have different scales.

D), suggesting that near and far surround may share similar suppressive mechanisms.

Figure 11*A* shows the distribution of SI_{patch} and $SI_{annulus}$ across V1 layers. We found significantly stronger suppression (both SI_{patch} and $SI_{annulus}$) in V1 upper layers (4B and above) compared with suppression in deeper layers ($P < 0.001$ for both SI_{patch} and $SI_{annulus}$; Kruskal–Wallis test). This was attributed to a greater proportion of neurons in layers 4B and above having a $SI_{patch} > 0.6$ or a $SI_{annulus} > 3.5$; instead all cells in layers 5 and 6 had a $SI_{patch} \leq 0.6$ and most cells in these layers had a $SI_{annulus} < 0.35$. Layer 4C showed larger scatter in SIs compared with that in other layers. In contrast to V1, in V2 we found no significant laminar differences in the distribution of SIs (Fig. 11, *B* and *C*). Cells that were strongly and weakly suppressed by grating patches or annular gratings in the surround were found in all layers. However, there was a tendency for far surround suppression ($SI_{annulus}$) to be weaker in layer 6 (median $SI_{annulus}$ in layers 3, 4, and 5 was 0.25, 0.28, and 0.25, respectively, vs. 0.19 in layer 6; Fig. 11*C*). In addition, compared with other layers, layer 3 showed a larger number of cells with stronger far surround suppression (Fig. 11*C*).

We found no differences in SIs across CO stripes. Mean and median values of SIs for each stripe type are reported in Table 2. Only three cells in the thick stripes and one cell in the thin stripes, but zero cells in the pale stripes showed a $SI_{patch} = 0$. Cells with $SI_{annulus} = 0$, instead, were more numerous and were found in all stripe types.

Most previous studies that examined the incidence of surround suppression or end-stopping in the different CO stripes of V2 have reported percentages of recorded cells in each stripe type that were end-stopped (summarized in Table 4 in Shipp and Zeki 2002a). To enable comparison of our data with data from these previous studies, we have calculated the percentage

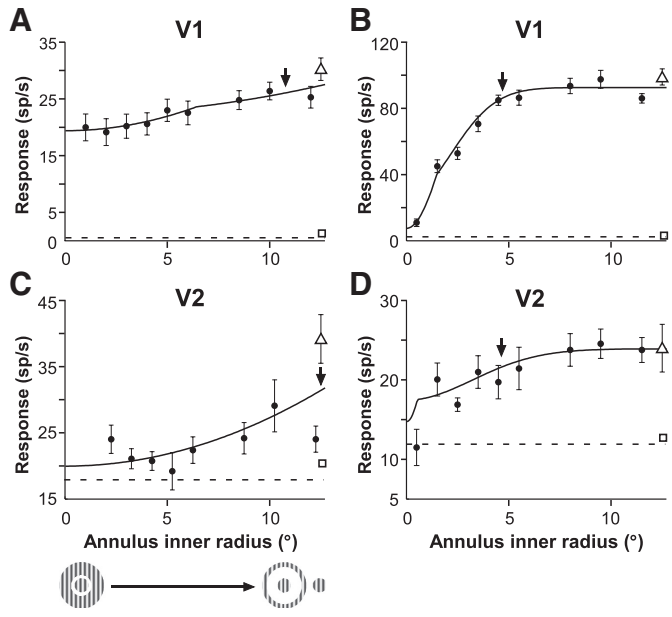

FIG. 7. Annulus-size tuning curves for 2 example V1 cells and 2 example V2 cells. Response of 2 V1 cells (*A* and *B*) and 2 V2 cells (*C* and *D*) as a function of the inner radius of an annular grating in the far surround (stimulus shown in *C*). Cells in *A* and *B* are the same cells shown in Fig. 2, *A* and *B*; *C* and *D* are the same cells as in Fig. 2, *D* and *E*. The open triangle represents the response to the center-only stimulus. Open square: response to the largest surround-only stimulus. Solid lines represent fits to the data using the thresholded (t)-DOG model (see METHODS). Arrows indicate the annulus inner radius at suppression onset, used as a measure of far surround size (10.4° in *A*, 4.3° in *B*, >12.5° in *C*, 4.2° in *D*). Note that in *C* suppression is already present at the largest annulus inner radius used. Dashed line: mean spontaneous firing rate. The SI measured with the annulus method at high stimulus contrast for each cell was: 31% (*A*), 61% (*B*), 40% (*C*), 23% (*D*).

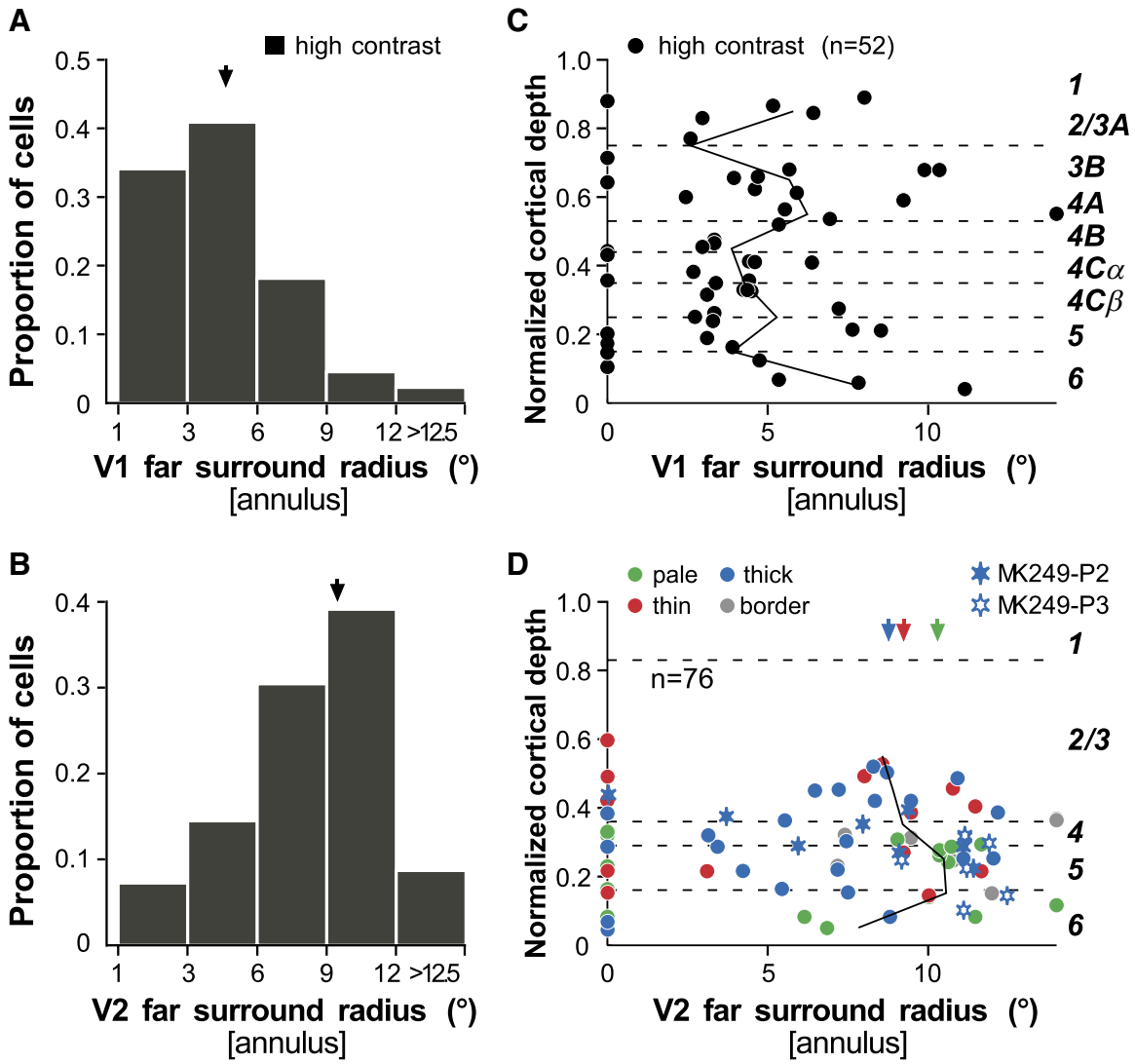

FIG. 8. Far surround sizes in V1 and V2 measured with expanding annulus method. *A* and *B*: distribution of far surround radii (annulus inner radius at suppression onset), measured at high contrast for the V1 (*A*) and V2 (*B*) cell samples. Maximum surround size of >12.5 ° indicates that the cell was suppressed by the largest annulus inner radius used. *C* and *D*: laminar distribution of far surround radii in V1 and V2, respectively. Other conventions are as in Fig. 4. Cells that showed no far surround suppression are indicated on the *y*-axes as cells having far surround radii = 0°. These cells were not included in the calculation of the median values (solid lines).

of cells in each stripe type having a SI_{patch} >0.5. By this criterion, 75% of cells in thick (30 of 40 cells) and pale (12 of 16 cells) stripes were surround suppressed versus 57% (8 of 14 cells) in thin stripes. For far surround suppression, we used as criterion of $SI_{annulus}$ >0.3 to classify a cell as surround suppressed because the SI >0.5 criterion would have excluded most cells in our sample (see Fig. 11*C*). Using the SI >0.3 criterion, 40% (16 of 40) of cells in thick stripes, 28.6% (4 of 14 cells) in thin stripes, and 12.5% (2 of 16 cells) in pale stripes showed far surround suppression.

Additional analyses of physiological response properties across V2 stripes

CLUSTER ANALYSIS. Our analysis of V2 data described earlier showed no statistically different distribution across stripe types for any of the main physiological response properties examined in this study. Because definition of V2 CO stripes as thin, thick, or pale was based on qualitative observation of CO staining density, width, and alternation, it is prone to errors. To identify objectively (i.e., independent of stripe assignment) any possible clustering of response properties in different V2 stripes, we performed a cluster analysis (see METHODS). The latter was performed on the following physiologically measured parameters: sRF_{high}, surround radius measured with expanding patch and annulus methods, and strength of surround suppression measured with expanding patch method (or SI_{patch}). For each of these parameters, the Thorndike procedure suggested a cluster size of 1, indicating homogeneity in the data set. This analysis confirmed lack of clustering in the RF and surround properties of V2 cells examined in this study.

STATISTICAL ANALYSIS OF STRIPE DIFFERENCES IN LAYERS 3/4 VERSUS 5/6. The statistical analyses described earlier testing for stripe differences in RF and surround properties were performed on the entire population of cells within each stripe type, pooled across V2 layers. However, previous studies have indicated that

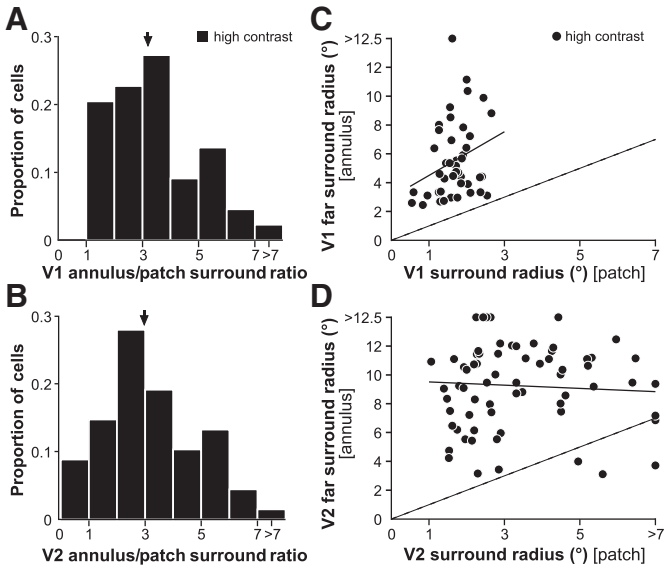

FIG. 9. Comparison of surround sizes measured with expanding annulus vs. expanding patch methods. *A* and *B*: distribution of the ratio of far surround size measured with expanding annulus to surround size measured with expanding patch in V1 (*A*; $n = 44$ cells) and V2 (*B*; $n = 69$ cells). Arrows indicate median values. *C* and *D*: scatterplots of far surround radius measured with annulus vs. surround radius measured with patch for the same V1 and V2 cell populations, respectively. In *C* and *D* all or most cells, respectively, lie above the diagonal (dashed line), indicating larger far surround sizes measured with the expanding annulus method. Continuous black lines in *C* and *D*: regression lines.

the characteristic properties of any given stripe type are more pronounced in V2 layers 3 and 4 (Shipp and Zeki 2002a; Shipp et al. 2009). Therefore we also performed the same statistical analysis reported earlier, but separately for the layer 3/4 and 5/6 cell populations. This analysis also revealed homogeneity across stripe types for all parameters examined. Specifically, we found no significant difference (Kruskal–Wallis test) across

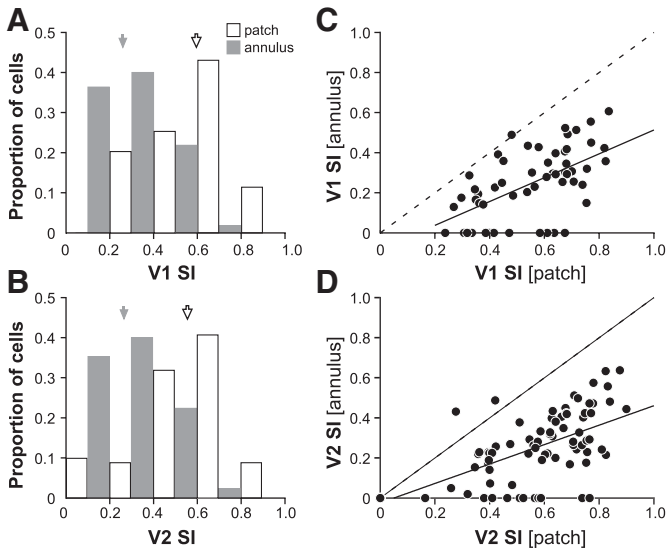

FIG. 10. Suppression indices (SIs) in V1 and V2. *A* and *B*: distribution of SI computed from the patch-size tuning (SI_{patch}) and annulus-size tuning ($SI_{annulus}$) data, for V1 (*A*) and V2 (*B*) cells. Gray and open arrows: median $SI_{annulus}$ and SI_{patch}, respectively (values reported in Table 1). *C* and *D*: scatterplots of SI_{patch} vs. $SI_{annulus}$, for the V1 and V2 cell populations, respectively. Almost all cells are below the diagonal, indicating larger SI_{patch} than $SI_{annulus}$ for most cells. Continuous black lines in *C* and *D*: regression lines.

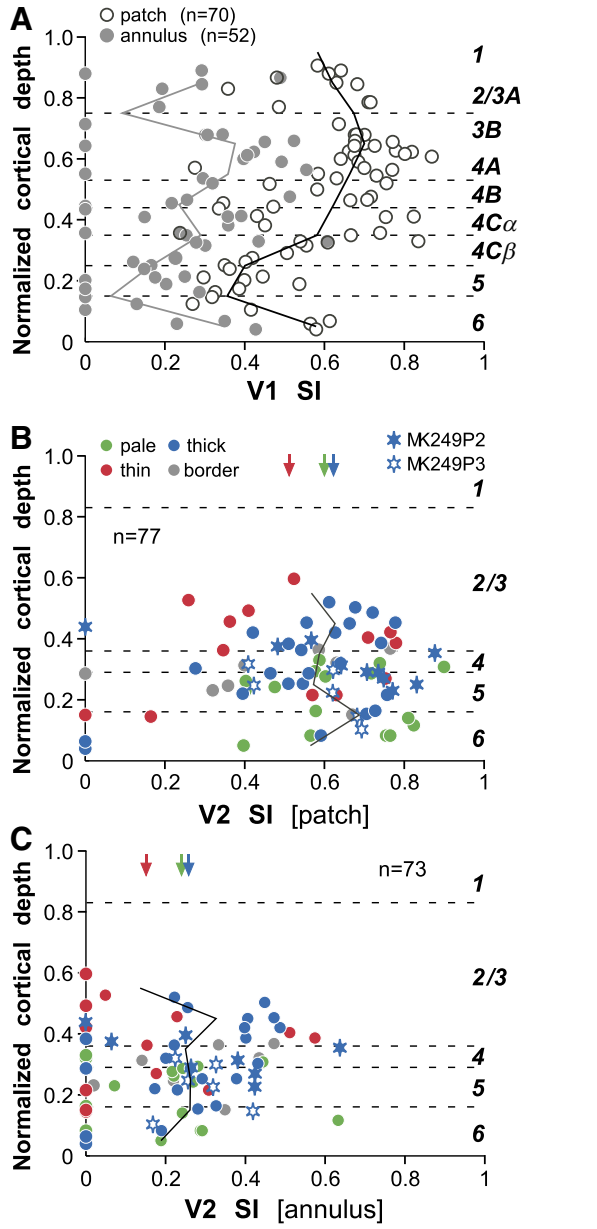

FIG. 11. Laminar distribution of SIs in V1 and in the V2 CO stripes. *A*: laminar distribution of SI_{patch} (open symbols) and $SI_{annulus}$ (gray symbols) for the V1 cell population. *B* and *C*: laminar distribution of SI_{patch} (*B*) and $SI_{annulus}$ (*C*) for the V2 cell population. Solid lines: median SI at intervals of 10% total cortical depth. Arrows: medians SIs for each stripe type pooled across layers (see Table 2 for values). Cells that showed no surround suppression (i.e., with a SI = 0) are indicated on the *y*-axes and were included in the calculation of the median values (both solid lines and arrows). Other conventions as in Fig. 4.

stripe types for the layers 3/4 or 5/6 cell populations in sRF_{high} radius ($P = 0.99$ and 0.17, respectively), surround size measured with expanding grating patches ($P = 0.82$ and 0.73, respectively), far surround size measured with expanding annular gratings ($P = 0.45$ and 0.81, respectively), SI_{patch} ($P = 0.34$ and 0.61, respectively), and $SI_{annulus}$ ($P = 0.31$ and 0.64, respectively).

Finally, to exclude that the lack of any significant laminar or CO stripe variation in many of the parameters examined, especially in V2, did not result from pooling of cells recorded

at different eccentricities, we examined whether the size of the sRF and surround (measured with expanding grating patches or annular gratings) and the strength of surround suppression (SI) varied with retinal eccentricity. Supplemental Fig. S1 shows that, with the exception of far surround size in V1, all other measured parameters in V1 and V2 were not significantly correlated with eccentricity.[1] However, because far surround radius in V1 was significantly correlated with eccentricity (Supplemental Fig. S1*E*; $r = 0.49$, $P = 0.001$), we asked whether the finding of smaller far surround radii in layer 4C (Fig. 8*C*) could be attributed to the smaller eccentricities of the receptive fields sampled in this layer. Supplemental Fig. S1*E* shows that this was not the case, given that our layer 4C cell sample (empty circles) spanned almost the full range of eccentricities of our entire V1 sample.

DISCUSSION

We quantitatively compared the spatial summation properties of V1 and V2 neuronal populations recorded in the same macaques. We found the RF and surround of V2 neurons to be a scaled version of those in V1. Both sRF and surround sizes in V2 were about twofold as large as those in V1. In both areas, the size of the sRF approximately doubled at low stimulus contrast. In V1 and V2, surround fields were about fivefold the size of the sRF, whereas the far surround, measured with the annulus method, was about threefold the size of the surround measured with the patch method. The strength of surround suppression was also similar in both areas. Similarities in the properties of RF and surround between the two areas suggest similar underlying mechanisms. The spatial scale of V2 surrounds suggests that, as in V1, interareal feedback connections to V2 likely underlie the far surround of V2 neurons.

We also examined the spatial properties of RF and surround in different V1 and V2 layers and in different V2 CO stripes. In V1, far surrounds were significantly larger outside input layer 4C and surround suppression was strongest in layers 4B and above. Thus in V1 there is a relation between stronger and larger suppressive surrounds and the laminar location of long-range intracortical connections (both horizontal and feedback). In V2, there is a conservation of all measured parameters across the various layers and stripe compartments. Thus the different parallel pathways through V2 do not differ in magnitude or spatial extent of surround suppression.

Summation receptive field

In V1, RF size was previously shown to depend on the stimulus and method used to measure it (Angelucci et al. 2002; Cavanaugh et al. 2002; Levitt and Lund 2002; Walker et al. 2000). Specifically, summation measurements made using expanding grating patches yield larger estimates of RF size (sRF) than measurements of minimum response field (Barlow et al. 1967). Furthermore, the sRF is larger when measured at low stimulus contrast (Sceniak et al. 1999; Sengpiel et al. 1997). Thus to measure the full extent of the excitatory RF region in V2 and compare it to that in V1, we performed spatial summation experiments and estimated the size of the sRF at both high and low contrast. Consistent with previous studies of spatial summation in V1, mean sRF_{high} radius for our V1 cell population was 0.36° (Cavanaugh et al. 2002; Levitt and Lund 2002; Sceniak et al. 2001; Solomon et al. 2004).

Mean sRF radius in V2 (0.74°) was about twofold that in V1, similar to that reported in two previous studies of spatial summation in macaque V2 (Solomon et al. 2004; Zhang et al. 2005). All other previous studies used the mRF as a measure of RF size and therefore reported values smaller than those in our study [e.g., a mean RF radius of 0.3° at 2–5° eccentricity was reported by Roe and Ts'o (1995)].

In both V1 and V2, sRF size increased by 1.7- and 1.6-fold, respectively, at low stimulus contrast. Contrast dependence of sRF size was previously demonstrated for V1 neurons (Cavanaugh et al. 2002; Sceniak et al. 1999; Sengpiel et al. 1997) and here we report it also for V2 neurons. Previously, we proposed that in V1 horizontal connections targeting excitatory cells and high-threshold, high-gain local inhibitory neurons could provide a mechanism for the contrast dependence of sRF size (Schwabe et al. 2006).

Contrast-dependent sRF size in V2 could be partially inherited from V1. However, the size of V1 cells sRF_{low} is about half that of V2 cells. Therefore additional intra-V2 mechanisms must play a role. Studies on the visuotopic extent of V2 horizontal connections are lacking. However, we can convert the size of the V2 sRF radii (Table 1) into cortical distances, using published measurements of cortical magnification factor across the CO stripes (Shipp and Zeki 2002b; 2.5 mm/deg at 5° eccentricity). Accordingly, sRF_{high} and sRF_{low} *diameters* in V2 would extend on average about 3.7 and 5 mm, respectively, across stripes. Figure 3*B* indicates that for a significant fraction (~35%) of cells, sRF_{low} diameters are larger than the mean values and would thus extend between 5 and 10 mm across stripes. Using injections of the neuroanatomical tracer biocytin into V2, Levitt et al. (1994b) demonstrated horizontal connections ≤8 mm in diameter across stripes. Using cholera toxin B, we found even longer horizontal connections in V2, ≤11 mm across stripes (Angelucci et al. 1998; Lund et al. 1999). Therefore horizontal V2 connections represent a feature of cortical anatomy that matches well the size of the sRF_{low} of V2 cells and may thus contribute to the generation of the V2 cortical RF.

Spatial extent of the suppressive surround

We used two different stimulus protocols to measure surround size: the expanding patch and the expanding annulus methods. The former stimulus activates all surround regions, both near and far, but it predominantly reveals the stronger suppressive effects arising from the near surround. In the latter stimulus protocol, only the far surround, but not the near surround, was stimulated.

Using the expanding patch method, and in agreement with previous studies (Cavanaugh et al. 2002; Levitt and Lund 2002; Sceniak et al. 2001; Solomon et al. 2004), the mean surround radius in V1 was 1.6° (reaching up to ~3°). Surround size measured using the expanding annulus method was about threefold larger than that when measured using the expanding patch method, averaging 5.5° (up to >12.5°). This is because masking out the stronger suppressive near surround allowed us to reveal weaker influences from the far surround.

Surround radii in V2 were about twofold larger than those in V1, averaging 3.6° (≤10.6°) when measured using the patch

[1] The online version of this article contains supplemental data.

method and 9.2° (up to >12.5°) when measured using the annulus method. Two previous studies (Solomon et al. 2004; Zhang et al. 2005) measured surround size in V2 using a stimulus protocol similar to our expanding patch method. Solomon et al. (2004) reported a smaller mean surround size, but they used smaller stimuli and a different measure of surround size than those used in our study. Instead, Zhang et al. (2005) reported much larger surround sizes in V2 (mean radius: ~7°) and described a population of special V2 neurons having exceptionally large surrounds (>6.5° and up to ~20° radius) and very strong surround suppression. However, these authors did not use grating patches >7.5° in radius for their spatial summation measurements and surround sizes larger than the largest presented stimulus were extrapolated from DOG model fits to a projected plateau. In contrast, in our study the largest measured surrounds corresponded to the cell's actual response to the largest presented grating patch.

We have previously proposed that far surround suppression in V1 neurons is mediated by extrastriate feedback connections to V1 and near surround suppression by feedforward and horizontal connections (Angelucci and Bressloff 2006; Angelucci et al. 2002; Schwabe et al. 2006). V2 surrounds must be, at least in part, inherited from V1. However, the much larger surround sizes in V2 than those in V1 and the narrow spread of feedforward V1-to-V2 connections (Lund et al. 1999; Salin and Bullier 1995; Salin et al. 1992) suggest a role for additional mechanisms operating within and/or beyond V2. Using published measurements of cortical magnification factor in V2, we can estimate that mean surround *diameters* in V2 (7.1 and 18.5°; see Table 1) correspond to cortical distances of about 17–46 mm—i.e., far longer than the extent of monosynaptic horizontal connections in V2. Therefore it is likely that in V2, as in V1, interareal feedback connections generate the larger far surrounds. The larger size of surrounds in V2 than in V1 could be accounted for by heavier feedback projections to V2, than to V1, from areas MT and V4 (Kennedy and Bullier 1985; Stepniewska et al. 2005; Ungerleider et al. 2008) (the largest feedback fields in V1 are from MT and they constitute a small fraction of all extrastriate feedback to V1; Angelucci et al. 2002). Furthermore compared with V1, V2 receives additional and/or heavier projections from higher-order parietal and temporal cortical areas having larger RFs than MT and V4 (Gattass et al. 1997; Perkel et al. 1986; Stepniewska and Kaas 1996).

Strength of surround suppression

Similar to two previous studies (Sceniak et al. 2001; Solomon et al. 2004), using expanding grating patches we found a mean suppression index (SI) in V1 of 0.58. Levitt and Lund (2002; median SI: 0.33) and Cavanaugh et al. (2002; mean SI: 0.38) reported weaker average suppression in V1. Differences in suppression strength across studies may partly depend on different sampling and/or depth of anesthesia. Previous studies reported that 11 to 40% of V1 cells (depending on the study) show no surround suppression (Cavanaugh et al. 2002; Levitt and Lund 2002; Sceniak et al. 2001; Solomon et al. 2004). In contrast, we found no V1 cells with SI <0.2 at high contrast. This may partly depend on our small sample of cells in layer 6, where most nonsuppressive cells are typically found (Cavanaugh et al. 2002; Levitt and Lund 2002; Sceniak et al. 2001).

Mean suppression strength for our V2 sample (mean SI = 0.54) was very similar to that for our V1 sample and the distributions of surround strengths were statistically indistinguishable between the two areas. Solomon et al. (2004) and Zhang et al. (2005) reported stronger average suppression in V2 (median and mean SI = 0.7) than that in V1. Again, differences among studies may depend on sampling biases and/or depth of anesthesia. However, Zhang et al. (2005) used much smaller stimulus sizes (7.5° largest grating radius) than those used in our study and suppression strength was estimated from DOG model fits extrapolated to a projected plateau. Our larger stimuli enabled a more precise estimation of V2 cell responses at larger stimulus sizes and provided more data points for statistical model fits.

For most V1 and V2 cells, the strength of far surround suppression measured with expanding annular gratings was weaker than that when measured with expanding grating patches (see also Solomon et al. 2004). However, mean strength of far surround suppression was very similar in V1 and V2 and the distributions of far suppression strengths in the two areas were statistically indistinguishable.

Cortical laminae and V2 stripe compartments

In V1, we found significant laminar differences only in the spatial extent of far surround suppression and in suppression strength, but no laminar differences in all other examined parameters. V1 surround sizes measured with expanding gratings showed no laminar variation, which is consistent with previous studies (Cavanaugh et al. 2002; Levitt and Lund 2002; Sceniak et al. 2001), although Sceniak et al. (2001) found that layer 6 cells had significantly larger surrounds than layer 2/3 cells. However, using the expanding annulus method and confirming our previous finding (Ichida et al. 2007), we found significantly smaller far surround sizes in V1 input layer 4C. The largest far surrounds that we measured in this layer were coextensive with the largest suppressive surrounds previously reported for macaque LGN (Alitto and Usrey 2008; Sceniak et al. 2006). These laminar differences in far surround size suggest that layer 4C neurons may inherit their surrounds from LGN afferents, whereas larger surrounds are generated within the V1 layers (2/3 and 5/6) that have long-range intracortical (horizontal and feedback) connections. Consistent with Sceniak et al. (2001), surround suppression in V1, measured with either method, was significantly stronger in the upper layers (4B and above). Thus in V1 there seems to be a correlation between stronger surrounds and the location of horizontal connections, which are more prominent and more specifically patterned in the upper layers than in layers 5/6 (Li et al. 2003; Lund et al. 2003; Rockland and Lund 1983). Feedback connections to V1, which we have proposed mediate the far surround, terminate in both upper and lower layers (Angelucci et al. 2002; Felleman and Van Essen 1991; Rockland and Pandya 1979), but may act by modulating horizontal connections to RF center neurons (Schwabe et al. 2006).

In V2, we found no laminar or CO stripe differences in any of the parameters we examined. We observed a small tendency for sRF sizes to be larger in layer 6 (consistent with Peterhans and von der Heydt 1993) and in the thin stripes (as previously reported by Roe and Ts'o 1995). Larger surround sizes dominated outside the input layers (3B–4) and in the pale stripes

and stronger far surrounds were found in layer 3, but these tendencies were all statistically nonsignificant. What is remarkable is the homogeneity of RF and surround properties across CO stripes, which was also confirmed by a cluster analysis. It has been suggested (Shipp and Zeki 2002a) that in V2, neurons in the middle layers show diversity in their properties, whereas the feedback receiving upper (2) and lower (5–6) layers shows homogeneity. However, our statistical analysis of stripe differences in RF and surround properties limited to the cells in layers 3–4 or 5–6 also showed no significant differences across CO stripe compartments. Several previous studies examined the incidence of end-stopping in the different CO stripes of macaque V2. Although all studies found end-stopping in all stripe types, its prevalence in different stripe types varied across studies, from dominating in pale stripes (Gegenfurtner et al. 1996; Peterhans and von der Heydt 1993) to prevailing in thin stripes (Levitt et al. 1994a; Shipp and Zeki 2002a) or in thick and pale stripes (Roe and Ts'o 1995; this study). However, in contrast to the present study, in all previous studies, but one (Gegenfurtner et al. 1996), end-stopping was defined qualitatively and in most of them no statistical analysis was performed to assess for significant differences across CO stripes in the incidence of end-stopping. The few studies that performed statistical tests (Gegenfurtner et al. 1996; Peterhans and von der Heydt 1993) reported, like our study, no significant stripe differences in the incidence of end-stopping.

We conclude that, despite the well-documented differences between stripe compartments with regard to many visual stimulus characteristics, homogeneity is maintained for the spatial extent and strength of suppression. This suggests that the basic circuit for surround suppression is maintained across V2, over which tuning to specific stimulus characteristics is superimposed.

ACKNOWLEDGMENTS

We thank K. Sainsbury for expert histological assistance, Dr. Lars Schwabe for advice regarding data analysis, and Dr. Zong-Xiang Tang for help with some experiments.

GRANTS

This work was supported by National Science Foundation Grants IBN-0344569 and IOS-0848106 to A. Angelucci, National Eye Institute Grants EY-015262 to A. Angelucci and EY-015609 to J. M. Ichida, National Center for Research Resources Grant 5G12 RR-03060 to J. B. Levitt, Wellcome Trust Grant 061113, and a Research to Prevent Blindness grant to the Department of Ophthalmology, University of Utah.

REFERENCES

Alitto HJ, Usrey WM. Origin and dynamics of extraclassical suppression in the lateral geniculate nucleus of the macaque monkey. *Neuron* 57: 135–146, 2008.

Allman J, Miezin F, McGuinness E. Stimulus specific responses from beyond the classical receptive field: neurophysiological mechanisms for local-global comparisons in visual neurons. *Ann Rev Neurosci* 8: 407–430, 1985.

Angelucci A, Bressloff PC. Contribution of feedforward, lateral and feedback connections to the classical receptive field center and extra-classical receptive field surround of primate V1 neurons. *Prog Brain Res* 154: 93–120, 2006.

Angelucci A, Levitt JB, Walton E, Hupé JM, Bullier J, Lund JS. Circuits for local and global signal integration in primary visual cortex. *J Neurosci* 22: 8633–8646, 2002.

Angelucci A, Lund JS, Walton E, Levitt JB. Retinotopy of connections within and between areas V1 to V5 of macaque visual cortex. *Soc Neurosci Abstr* 24: 897, 1998.

Angelucci A, Sainsbury K. Contribution of feedforward thalamic afferents and corticogeniculate feedback to the spatial summation area of macaque V1 and LGN. *J Comp Neurol* 498: 330–351, 2006.

Bair W, Cavanaugh JR, Movshon JA. Time course and time–distance relationships for surround suppression in macaque V1 neurons. *J Neurosci* 23: 7690–7701, 2003.

Barlow HB, Blakemore C, Pettigrew JD. The neural mechanisms of binocular depth discrimination. *J Physiol* 193: 327–342, 1967.

Blakemore C, Tobin EA. Lateral inhibition between orientation detectors in the cat's visual cortex. *Exp Brain Res* 15: 439–440, 1972.

Briggs F, Callaway EM. Laminar patterns of local excitatory input to layer 5 neurons in macaque primary visual cortex. *Cereb Cortex* 15: 479–488, 2005.

Cauli B, Porter JT, Tsuzuki K, Lambolez B, Rossier J, Quenet B, Audinat E. Classification of fusiform neocortical interneurons based on unsupervised clustering. *Proc Natl Acad Sci USA* 97: 6144–6149, 2000.

Cavanaugh JR, Bair W, Movshon JA. Nature and interaction of signals from the receptive field center and surround in macaque V1 neurons. *J Neurophysiol* 88: 2530–2546, 2002.

Chen G, Lu HD, Roe AW. A map for horizontal disparity in monkey V2. *Neuron* 58: 442–450, 2008.

DeAngelis GC, Freeman RD, Ohzawa I. Length and width tuning of neurons in the cat's primary visual cortex. *J Neurophysiol* 71: 347–374, 1994.

DeYoe EA, Felleman DJ, Van Essen DC, McClendon E. Multiple processing streams in occipitotemporal visual cortex. *Nature* 371: 151–154, 1994.

DeYoe EA, Van Essen DC. Segregation of efferent connections and receptive field properties in visual area V2 of the macaque. *Nature* 317: 58–61, 1985.

Federer F, Ichida JM, Jeffs J, Angelucci A. Multiple output pathways from V1 layer 4B to V2 CO stripes. *2008 Abstracts Viewer/Itinerary Planner*. Washington, DC: Society for Neuroscience.

Felleman DJ, Van Essen DC. Distributed hierarchical processing in the primate cerebral cortex. *Cereb Cortex* 1: 1–47, 1991.

Felleman DJ, Xiao Y, McClendon E. Modular organization of occipitotemporal pathways: cortical connections between visual area 4 and visual area 2 and posterior inferotemporal ventral area in macaque monkeys. *J Neurosci* 17: 3185–3200, 1997.

Gattass R, Sousa AP, Mishkin M, Ungerleider LG. Cortical projections of area V2 in the macaque. *Cereb Cortex* 7: 110–129, 1997.

Gegenfurtner KR, Kiper DC, Fenstemaker SB. Processing of color, form, and motion in macaque area V2. *Vis Neurosci* 13: 161–172, 1996.

Gilbert CD, Wiesel TN. The influence of contextual stimuli on the orientation selectivity of cells in primary visual cortex of the cat. *Vision Res* 30: 1689–1701, 1990.

Girard P, Hupé JM, Bullier J. Feedforward and feedback connections between areas V1 and V2 of the monkey have similar rapid conduction velocities. *J Neurophysiol* 85: 1328–1331, 2001.

Hubel DH, Livingstone MS. Segregation of form, color, and stereopsis in primate area 18. *J Neurosci* 7: 3378–3415, 1987.

Ichida JM, Schwabe L, Angelucci A. Contrast dependence of "far" surround suppression in macaque V1. *2007 Abstracts Viewer/Itinerary Planner*. Washington, DC: Society for Neuroscience CD-ROM.

Ichida JM, Schwabe L, Bressloff PC, Angelucci A. Response facilitation from the "suppressive" receptive field surround of macaque V1 neurons. *J Neurophysiol* 98: 2168–2181, 2007.

Kapadia MK, Westheimer G, Gilbert CD. Dynamics of spatial summation in primary visual cortex of alert monkeys. *Proc Natl Acad Sci USA* 96: 12073–12078, 1999.

Kennedy H, Bullier J. A double-labeling investigation of the afferent connectivity to cortical area V1 and V2 of the macaque monkey. *J Neurosci* 5: 2815–2830, 1985.

Levitt JB, Kiper DC, Movshon JA. Receptive fields and functional architecture of macaque V2. *J Neurophysiol* 71: 2517–2542, 1994a.

Levitt JB, Lund JS. The spatial extent over which neurons in macaque striate cortex pool visual signals. *Vis Neurosci* 19: 439–452, 2002.

Levitt JB, Yoshioka T, Lund JS. Intrinsic cortical connections in macaque visual area V2: evidence for interaction between different functional streams. *J Comp Neurol* 342: 551–570, 1994b.

Li H, Fukuda M, Tanifuji M, Rockland KS. Intrinsic collaterals of layer 6 Meynert cells and functional columns in primate V1. *Neuroscience* 120: 1061–1069, 2003.

Lu HD, Roe AW. Functional organization of color domains in V1 and V2 of macaque monkey revealed by optical imaging. *Cereb Cortex* 18: 516–533, 2008.

Lund JS, Angelucci A, Bressloff PC. Anatomical substrates for functional columns in macaque monkey primary visual cortex. *Cereb Cortex* 13: 15–24, 2003.

Lund JS, Angelucci A, Walton EJS, Bullier J, Hupé J-M, Girard P, Levitt JB. Topographic logic of connections within and between macaque monkey visual cortical areas V1, V2, V3, and V5. *Invest Ophthalmol Vis Sci* 40: S645, 1999.

Nakamura H, Gattass R, Desimone R, Ungerleider LG. The modular organization of projections from areas V1 and V2 to areas V4 and TEO in macaques. *J Neurosci* 13: 3681–3691, 1993.

Nelson JI, Frost B. Orientation selective inhibition from beyond the classical receptive field. *Brain Res* 139: 359–365, 1978.

Perkel DJ, Bullier J, Kennedy H. Topography of the afferent connectivity of area 17 in the macaque monkey: a double-labelling study. *J Comp Neurol* 253: 374–402, 1986.

Peterhans E, von der Heydt R. Functional organization of area V2 in the alert macaque. *Eur J Neurosci* 5: 509–524, 1993.

Rockland KS, Lund JS. Intrinsic laminar lattice connections in primate visual cortex. *J Comp Neurol* 216: 303–318, 1983.

Rockland KS, Pandya DN. Laminar origins and terminations of cortical connections of the occipital lobe in the rhesus monkey. *Brain Res* 179: 3–20, 1979.

Roe AW, Ts'o DY. Visual topography in primate V2: multiple representation across functional stripes. *J Neurosci* 15: 3689–3715, 1995.

Salin PA, Bullier J. Corticocortical connections in the visual system: structure and function. *Physiol Rev* 75: 107–154, 1995.

Salin PA, Kennedy H, Bullier J. Visuotopic organization of corticocortical connections in the visual system of the cat. *J Comp Neurol* 320: 415–434, 1992.

Sceniak MP, Chatterjee S, Callaway EM. Visual spatial summation in macaque geniculocortical afferents. *J Neurophysiol* 96: 3474–3484, 2006.

Sceniak MP, Hawken MJ, Shapley RM. Visual spatial characterization of macaque V1 neurons. *J Neurophysiol* 85: 1873–1887, 2001.

Sceniak MP, Ringach DL, Hawken MJ, Shapley R. Contrast's effect on spatial summation by macaque V1 neurons. *Nat Neurosci* 2: 733–739, 1999.

Schwabe L, Obermayer K, Angelucci A, Bressloff PC. The role of feedback in shaping the extra-classical receptive field of cortical neurons: a recurrent network model. *J Neurosci* 26: 9117–9129, 2006.

Sengpiel F, Baddley RJ, Freeman TCB, Harrad R, Blakemore C. Different mechanisms underlie three inhibitory phenomena in cat area 17. *Vision Res* 38: 2067–2080, 1998.

Sengpiel F, Sen A, Blakemore C. Characteristics of surround inhibition in cat area 17. *Exp Brain Res* 116: 216–228, 1997.

Shipp S, Adams DL, Moutoussis K, Zeki S. Feature binding in the feedback layers of area V2. *Cereb Cortex* (January 19, 2009). doi:10.1093/cercor/bhn243.

Shipp S, Zeki S. Segregation of pathways leading from area V2 to areas V4 and V5 of macaque monkey visual cortex. *Nature* 315: 322–325, 1985.

Shipp S, Zeki S. The functional organization of area V2, I. Specialization across stripes and layers. *Vis Neurosci* 19: 187–210, 2002a.

Shipp S, Zeki S. The functional organization of area V2, II. The impact of stripes on visual topography. *Vis Neurosci* 19: 211–231, 2002b.

Sincich LC, Horton JC. Divided by cytochrome oxidase: a map of the projections from V1 to V2 in macaques. *Science* 295: 1734–1737, 2002.

Sincich LC, Horton JC. The circuitry of V1 and V2: integration of color, form, and motion. *Annu Rev Neurosci* 28: 303–326, 2005.

Solomon SG, Peirce JW, Lennie P. The impact of suppressive surrounds on chromatic properties of cortical neurons. *J Neurosci* 24: 148–160, 2004.

Stepniewska I, Collins CE, Kaas JH. Reappraisal of DL/V4 boundaries based on connectivity patterns of dorsolateral visual cortex in macaques. *Cereb Cortex* 15: 809–822, 2005.

Stepniewska I, Kaas JH. Topographic patterns of V2 cortical connections in macaque monkeys. *J Comp Neurol* 371: 129–152, 1996.

Tamura H, Sato H, Katsuyama N, Hata Y, Tsumoto T. Less segregated processing of visual information in V2 than in V1 of the monkey visual cortex. *Eur J Neurosci* 8: 300–309, 1996.

Thorndike RL. Who belongs in the family? *Psychometrika* 18: 267–276, 1953.

Tootell RB, Hamilton SL. Functional anatomy of the second visual area (V2) in the macaque. *J Neurosci* 9: 2620–2644, 1989.

Tootell RB, Nelissen K, Vanduffel W, Orban GA. Search for color "center(s)" in macaque visual cortex. *Cereb Cortex* 14: 353–363, 2004.

Ts'o DY, Frostig RD, Lieke EE, Grinvald A. Functional organization of primate visual cortex revealed by high resolution optical imaging. *Science* 249: 417–420, 1990.

Ungerleider LG, Galkin TW, Desimone R, Gattas R. Cortical connections of area V4 in the macaque. *Cereb Cortex* 18: 477–499, 2008.

Vanduffel W, Tootell RB, Schoups AA, Orban GA. The organization of orientation selectivity throughout macaque visual cortex. *Cereb Cortex* 12: 647–662, 2002.

Walker GA, Ohzawa I, Freeman RD. Suppression outside the classical cortical receptive field. *Vis Neurosci* 17: 369–379, 2000.

Xiao Y, Felleman DJ. Projections from primary visual cortex to cytochrome oxidase thin stripes and interstripes of macaque visual area 2. *Proc Natl Acad Sci USA* 101: 7147–7151, 2004.

Xiao Y, Wang YI, Felleman DJ. A spatially organized representation of color in macaque cortical area V2. *Nature* 421: 535–439, 2003.

Xu X, Bosking W, Sary G, Stefansic J, Shima D, Casagrande V. Functional organization of visual cortex in the owl monkey. *J Neurosci* 24: 6237–6247, 2004.

Zhang B, Zheng J, Watanabe I, Maruko I, Bi H, Smith EL 3rd, Chino Y. Delayed maturation of receptive field center/surround mechanisms in V2. *Proc Natl Acad Sci USA* 102: 5862–5867, 2005.